ISSN : 0974 - 7486 Volume 12 Issue 11

Materials Science

An Indian Journal

Full Paper

MSAIJ, 12(11), 2015 [392-399]

Long time oxidation at 1000°c of a cast ni-25cr-0.5c alloy: determination of the kinetic constants and metallographic characterization of the oxidized state for the deduction of the chromium diffusion coefficient in subsurface

Elodie Conrath, Patrice Berthod*

Institut Jean Lamour (UMR 7198), Team 206 "Surface and Interface, Chemical Reactivity of Materials" University of Lorraine, Faculty of Sciences and Technologies B.P. 70239, 54506 Vandoeuvre-lès-Nancy, (FRANCE)

E-mail : patrice.berthod@univ-lorraine.fr

ABSTRACT

The diffusion of chromium in alloys, the oxidation resistance of which depends on their chromia-forming behaviour, is of great importance. After long times of oxidation such alloys are modified in subsurface by notably the development of a carbide-free zone which may significantly influence the diffusion of chromium. Diffusion coefficients red in handbooks for bulk alloys can thus be not efficient to correctly represent diffusion in these subsurfaces. In this work a method associating thermogravimetry measurements themselves and chromium concentration profiles acquired on cross sections prepared from the corresponding oxidized samples, was used to try specifying the chromium diffusion coefficient in this special alloy environment which is the subsurface of the oxidizing alloy itself. This led to a value of almost 3×10^{-11} cm^2 s^{-1} for 1000°C in the subsurface of a Ni-25Cr-0.5C alloy.

KEYWORDS

Nickel-based alloys;
Chromium carbides;
High temperature oxidation;
Thermogravimetry;
Post-mortem characterization;
Chromium diffusion coefficient.

INTRODUCTION

In metallic alloys exposed to high temperature the diffusion phenomena play very important role. This is true first for the different possible stage of their elaboration " as in powder metallurgy[1,2], mechanical alloying[3], joining / welding[4], deposition of coatings[5] or heat treatments[6] – and second during they are used. In the later case one can cite the chemical phenomena such as oxidation since it involves the diffusion of elements such as Al, Cr or Si [7,8]. Aluminum, chromium or silicon are usually present in superalloys[9,10] in quantities high enough for bringing an alumina-forming, chromia-forming or silica-forming behavior respectively, to the alloys when they are exposed to oxidant gases at high temperature. The contents in these elements are a first criterion indicating the oxidation resistance potential of these high temperature alloys; for example, in the case of chromium, 20 wt.% Cr in a nickel-based alloy and 30 wt.% Cr in a cobalt-based alloy are often considered as minimal contents. A second very important criterion is the easiness of diffusion of the considered element in the subsurface of the alloys. A sufficiently good diffusion of Al, Cr or Si towards the oxidation front is

necessary for obtaining the development and thereafter for maintaining a continuous protective scale of Al_2O_3, Cr_2O_3 and SiO_2 respectively. The values of diffusion coefficients of Al, Cr or Si are generally available only about the diffusion of these elements in pure metals or simple solid solutions. Unfortunately the use of these values in case of multi-phase alloys is often not evident. The knowledge of the average diffusion coefficients taking into account the influence of the grain orientation, the grain boundaries and the second phases possibly present interdendritically is though important to value the sustainability of the protecting effect of the considered element.

The thermogravimetry tests in hot oxidant gases, which are commonly used to evaluate the high temperature oxidation resistance, can be also used to characterize the diffusion of the most oxidable species existing in the alloys[11]. The association of the measurements of oxidation-induced mass gain by thermo-balance with the concentration profiles acquired in the sub-surface of the oxidized samples may effectively permitting the deduction of the global diffusion coefficients[11,12]. In the present study the diffusion of chromium was specified at 1000°C by this method for a cast polycrystalline alloy based on nickel and containing 25 wt.%Cr and 0.5 wt.%C.

EXPERIMENTAL DETAILS OF THE STUDY

Elaboration of the alloy of the study

The Ni(bal.)-25Cr-0.5C (all contents in weight percent) was initially elaborated by foundry. Pure nickel, pure chromium and graphite (Alfa Aesar, purity higher than 99.9 wt.%) were weighed and placed in the water-cooled copper crucible of a CELES furnace. Their heating was realized by high frequency induction under an inert atmosphere composed of 300 mbar of pure argon. The applied operating parameters " about 110 kHz and 4kV – allowed obtaining the molten alloy. This one was thereafter maintained at about 1600°C for three minutes to completely homogenize the melt. The power was then decreased to solidify it. The alloy entered in contact with the metallic crucible and cooled down to room temperature.

The obtained ingot, of a compact shape, was then cut to get a part for the observation of the as-cast microstructure and for the control of the obtained chemical composition. Another part was machined to get samples (parallelepipeds of about 8 mm × 8 mm × 3 mm) destined to be oxidized with thermogravimetry follow up of their mass change and thereafter to be analyzed for specifying the concentration profiles in their sub-surface.

The oxidation test

A parallelepipedic sample was machined using a Buehler Delta Abrasimet metallographic saw. It was ground on its six faces with 1200-grit SiC papers. Its edges and corners were smoothed by grinding them using the same papers. For performing the thermogravimetry test a SETARAM TG92 thermobalance was used. The test was carried out under a flow of synthetic dry air ($80\%N_2$-$20\%O_2$). Three successive stages composed the thermal cycle: a heating phase at +20K / min, an isothermal stage at T=1000°C for Δt=114h, and a cooling phase at -5K / min. This test led to a mass gain file {Δm/S = f(t)} whose isothermal part end was analyzed to value the final mass gain rate dm/dt before the start of cooling. This mass gain corresponds to the oxygen atoms which came on surface to be combined with the most oxidable element present in the alloy: Cr. One can write the following equation:

$$\left(\frac{dm}{dt}\right)_{end} = \frac{M_o}{S} \times \left(\frac{dn_o}{dt}\right)$$

where m is the mass gain per surface unit area (and $\left(\frac{dm}{dt}\right)_{end}$ the mass gain rate) at the end of the isothermal stage, M_o=16g × mol^{-1} the oxygen molar mass, and $\left(\frac{dn_o}{dt}\right)_{end}$ the number of oxygen moles initially present in air and arrived on the sample to be combined with metal to be added to the oxide scale.

By considering the main oxidation reaction ($2 \times Cr + \frac{3}{2} O_2 \rightarrow Cr_2O_3$), the number of moles of Cr diffusing from the alloy to be combined

Full Paper

with oxygen in the oxide scale, appears as equal to:

$$\left(\frac{dn_{Cr}}{dt}\right)_{end} = \frac{2}{3}\times\left(\frac{dn_{O}}{dt}\right)_{end} = \left(\frac{2\times S}{3\times M_{o}}\right)\times\frac{d\left(\frac{\Delta m}{S}\right)}{dt}_{end}$$

Characterization of the oxidized sample

After return to room temperature the oxidized sample was first subjected to X-ray diffraction (XRD) to specify the nature of the oxides formed on surface. This was done using a Philips X'Pert Pro diffractometer (λ=1.5406 Angström, Cu K_{α}). The oxidized sample was thereafter covered by a thin layer of gold deposited by cathodic evaporation, which allowed characterizing the oxide scale: using a Scanning Electron Microscope (SEM) JEOL JSM 6010LA in Secondary Electrons (SE) mode and composition analyze by using the Energy Dispersion Spectrometry (EDS) apparatus equipping this SEM.

The oxidized samples, became electrically conductivity by the previous gold deposition, were also electrolytically coated with a thick layer of nickel (cathodic polarization in a 50°C-heated Watt's bath). A Buehler Delta Abrasimet saw was used to cut it in two parts, without minimized loss of oxides since mechanically protected by the thick nickel shell surrounding it. The two parts were embedded in a cold resin mixture (Araldite CY230 resin with HY956 hardener, Escil) and ground with SiC papers from 240-grit to 1200-grit. After cleaning with ultrasounds the mounted sample was polished with textile enriched with 1µm hard particles.

Observations in cross-section were carried out with the SEM, in Back Scattered Electrons (BSE) mode. EDS spot analysis allowed specifying again the natures of the oxides. EDS was also involved in acquiring concentration profiles in the sub-surface, perpendicularly to the alloy/oxide interface of the alloy.

This allowed revealing a Cr- zone impoverished part in the subsurface. The chromium profile presented an almost linear shape over the chromium-depleted depth. This allowed the determination of the average gradient in chromium concentration C_{Cr}: $\left\|\overrightarrow{grad\ C_{Cr}}\right\|$ (expressed in mol × cm^{-4}):

$$\left\|\overrightarrow{\mathbf{grad\ C_{Cr}}}\right\| = \left(\frac{\rho_{alloy}}{M_{Cr}}\right)\times\frac{\Delta WCt_{Cr}}{\Delta h}$$

In which ρ_{alloy} is the density of the alloy (considered as being 8.9 g × cm^{-3}), M_{Cr} the molar mass of chromium (equal to 52g × mol^{-1}) and $\frac{\Delta WCt_{Cr}}{\Delta h}$ the average gradient of the weight content in chromium (z: depth).

Determination of the average diffusion coefficient for chromium

The previous data were finally used to calculate an estimated value of the average coefficient for chromium diffusion through the sub-surface, according to the Fick's first law:

$$\left(\frac{dn_{Cr}}{dt}\right)_{end} = -D_{Cr}\times\left\|\overrightarrow{\mathbf{grad\ C_{Cr}}}\right\|$$

By replacing $\left(\frac{dn_{Cr}}{dt}\right)_{end}$ and $\left\|\overrightarrow{grad\ C_{Cr}}\right\|$ by their expression previously given:

$$D_{Cr} = \left(\frac{2\times M_{Cr}}{3\times M_{O}}\right)\times\frac{\frac{dm}{dt}_{end}+K_{v}}{\rho_{all}\times\frac{\Delta WCt_{Cr}}{\Delta h}}$$

In this late expression K_v is the chromia volatilization constant which kinetically characterizes the linear loss of chromia Cr_2O_3, oxidized again and this time into an oxide, CrO_3, which is gaseous when temperature is higher than 1000°C. This constant was determined, as the parabolic constant K_p by plotting the mass gain results as $m\times\frac{dm}{dt} = f(-m)$, and by exploiting them according to the following equation, $m\times\frac{dm}{dt} = K_p + (-m)\times K_v$, method established in a previous work[13].

RESULTS AND DISCUSSION

The obtained mass gain curves

The obtained mass gain curve is presented in Figure 1. The kinetic oxidation regime is parabolic-type,

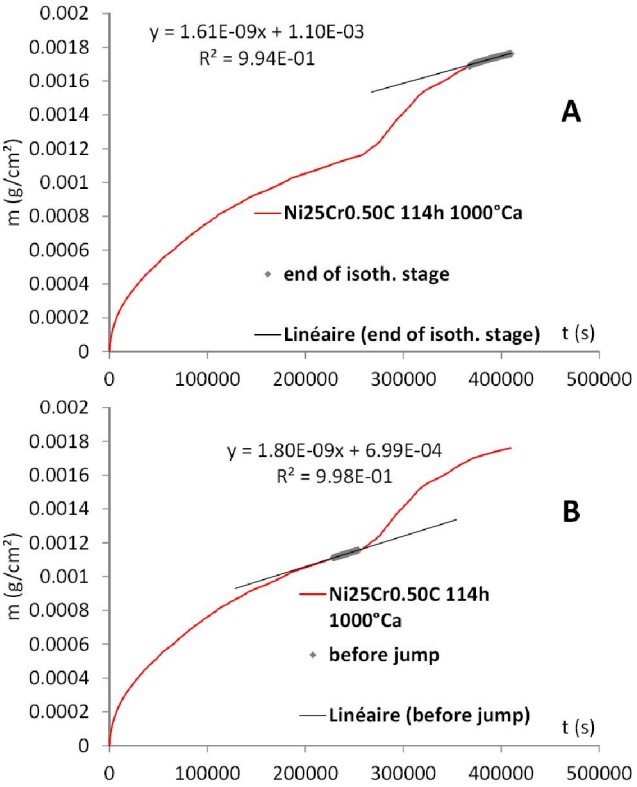

Figure 1 : Determination of the final mass gain rate at the end of the 114h-long 1000°C-isothermal stage for the Ni-25Cr-0.5C alloy in synthetic dry air

but the local problem of binding-unsticking of the external scale was obviously at the origin of the mass gain jump occurred at about 250,000 seconds. Since the total mass gain may be influenced thereafter by the local acceleration of oxidation resulting from the fast oxidation of the corresponding denuded part of alloy's surface, it was preferred to consider two mass gain rates, not only the one at the end of isothermal stage (A) but also the one existing just before the mass jump (B).

If the first value (16.1×10^{-10} g cm^{-2} s^{-1}, A) may be slightly modified by the mass gain jump occurred before, the second one (18.0×10^{-10} g cm^{-2} s^{-1}, B) is characteristic of the homogeneous Cr diffusion towards the oxidation front… but at t equal to 250,000 s: this will not correspond to the chromium gradient which will be specified through the subsurface zone depleted in Cr between = 0 and t = 410,400s (114h). It was finally preferred to keep the value measured at the end of the isothermal stage (16.1×10^{-10} g cm^{-2} s^{-1}, A).

The mass gain file was also treated according to the {} method[13] to specify the value of the volatilization constant (Figure 2). This one is 19.0×10^{-10} g cm^{-2} s^{-1}, as is to say of the same order of magnitude as (and even almost equal to!). The value obtained for the K_v constant as well as the one sobtained for the not underestimated K_p value are tested by reconstructing a mathematical curve (green) to compare with the experimental curve (Figure 3): it well fits this one, better than the red mathematical curve plotted by using only the K_p value which can be classically determined (as is to say without taking into account the mass loss due to chromia volatilization).

All these kinetic results, together with the value of K_p classically determined and the one issued from the treatment, are displayed in TABLE 1.

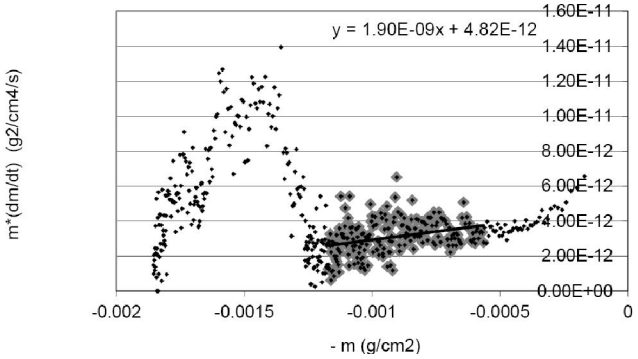

Figure 2 : Determination of the linear constant K_v (1.9×10^{-9} g cm^{-2} s^{-1}) characterizing the mass loss rate by volatilization of chromia (together with the K_p simultaneously determined: 4.82×10^{-12} g^2 cm^{-4} s^{-1})

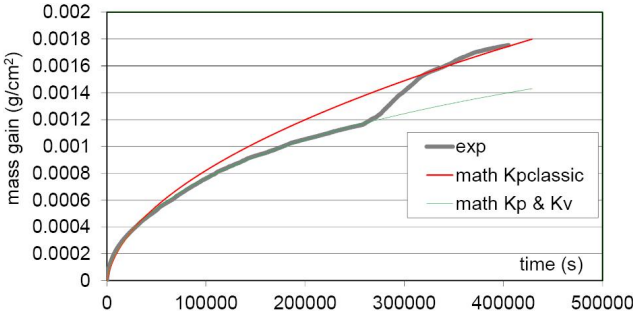

Figure 3 : Validation test of the values obtained for K_v (and K_p); much better correspondence than for the classically determined K_p value only

Characterization of the oxidized sample

After return to room temperature the sample has lost a part of its external oxide scale. This was first revealed by the plot of the mass gain file as mass gain versus temperature (after correction from the air buoyancy variation), leading to the curve presented in Figure 4. This one was also entirely exploited to get data about the temperature of oxidation start (defined as

Full Paper

TABLE 1 : Values of the different kinetic constants issued from the treatments of the mass gain files (in bold characters: the values finally taken into account)

Constant	Value	Unit
$\left(\frac{dm}{dt}\right)_{end}$ (A)	16.1×10^{-10}	g cm^{-2} s^{-1}
$\left(\frac{dm}{dt}\right)_{end}$ (B)	18.0×10^{-10}	g cm^{-2} s^{-1}
K_p (classical determination)	4.20×10^{-12}	g^2 cm^{-4} s^{-1}
K_p (by taking the chromia volatilization into account)	4.82×10^{-12}	g^2 cm^{-4} s^{-1}
K_v (chromia volatilization	19.0×10^{-10}	g cm^{-2} s^{-1}

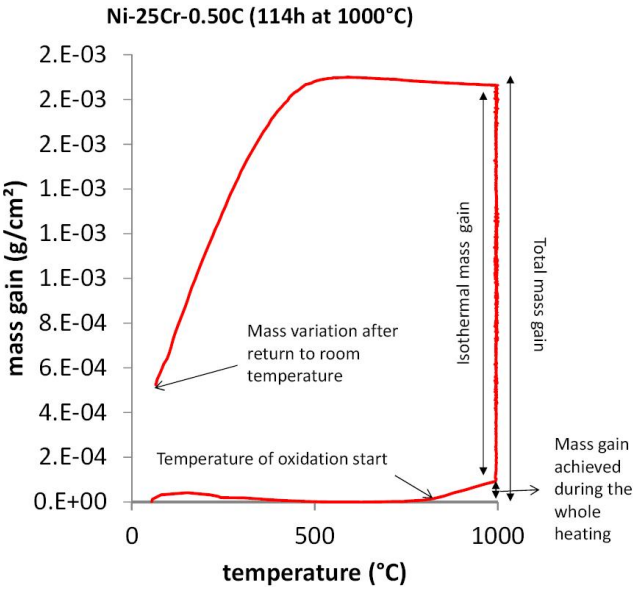

Figure 4 : Exploitation of the mass gain results obtained during the whole thermal cycle

being the temperature at which the mass gain by oxidation became to be significant enough to be detected by the used thermobalance (thus definition relative to the apparatus sensivity), the different mass gains (whole heating, isothermal mass gain, the two previous ones together, the temperature of oxide spallation start); the obtained results are all displayed in TABLE 2.

The part of external oxide scale remaining on the sample was specified by XRD analysis. The results show, as illustrated by the diffractogram shown in Figure 5, that chromia (Cr_2O_3) is the main oxide present, despite the presence of additional $NiCr_2O_4$ spinel oxide. This allowed considering that the formula established above may be effectively used for the determination of the diffusion coefficient of chromium.

The morphology and nature of the external oxide scale are illustrated in Figure 6 by a SEM micrograph taken in Secondary Electrons mode (topography, A) and a second one taken in Back Scattered Electrons mode (composition, B), for two different magnifications. The last one is enriched by EDS results (chromia, chromium in extreme surface measured on a totally denuded zone).

After the preparation of the cross-section sample new observations were carried out with the SEM in BSE mode. As illustrated by the SEM/BSE micrograph shown in Figure 7, one can see that a carbide-free zone was developing inwards from the oxide/interface. SEM/EDS concentration profiles were performed through the subsurface affected by oxidation, with as result the one given in Figure 8. One can see an almost linear variation in chromium content which increases from about 14 wt.% up to 21-22 wt.%Cr when reaching the frontier separating the carbide-free zone and the bulk. A

TABLE 2 : Values of the different characteristics resulting from the mass gain exploitation for the whole thermal cycle

Data	Part of the curve	Value
Temperature of oxidation start	heating	768.3°C
Mass gain achieved during the whole heating	heating	0.1017 mg cm^{-2}
Isothermal mass gain	isothermal stage	1.7613 mg cm^{-2}
Total mass gain	heating + isothermal stage	1.8630 mg cm^{-2}
Temperature of oxide scale spallation start	cooling	496.5°C
Total mass variation	Whole cycle	0.548 mg cm^{-2}

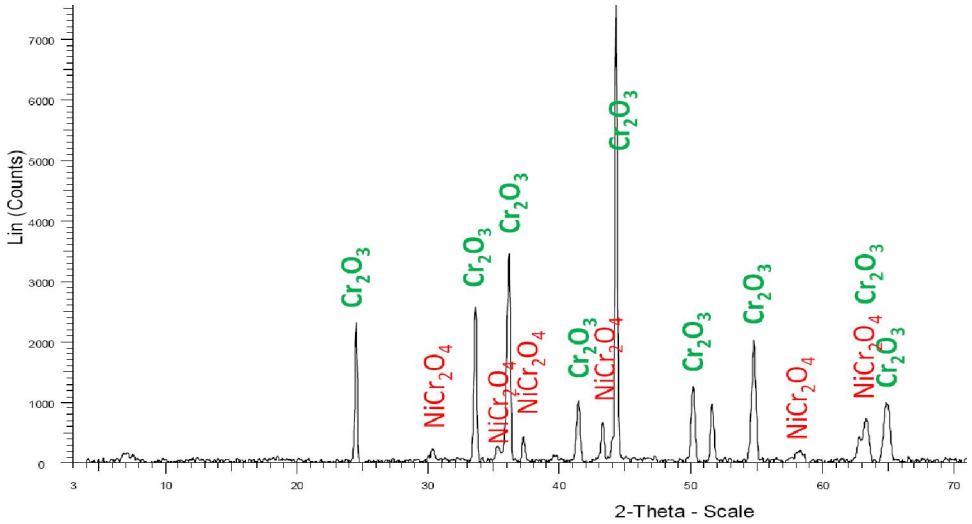

Figure 5 : XRD diffractogram acquired on the surface of the oxidized sample

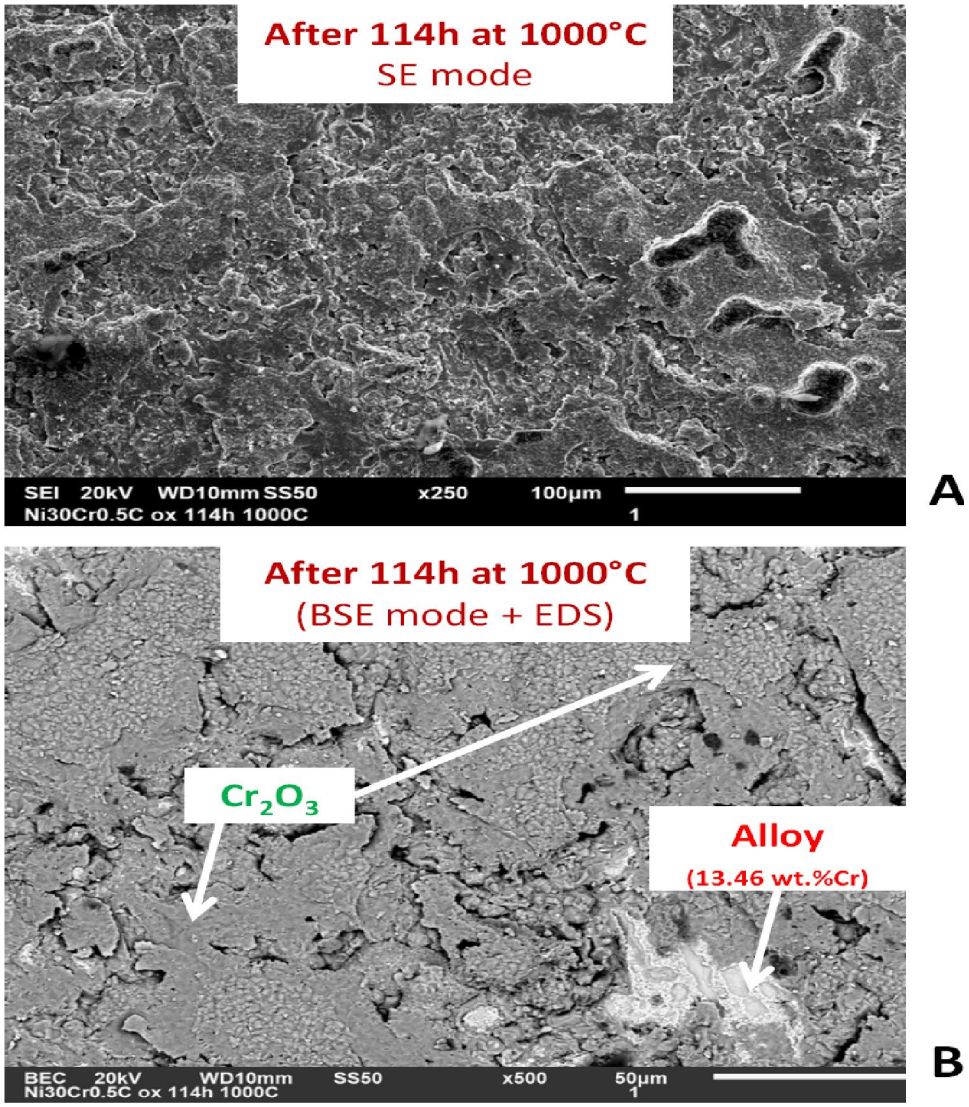

Figure 6 : SEM illustrating the external oxide scale (A: morphology at ×250 in SE mode, B: nature at ×1000 in BSE mode with EDS spot analysis)

Full Paper

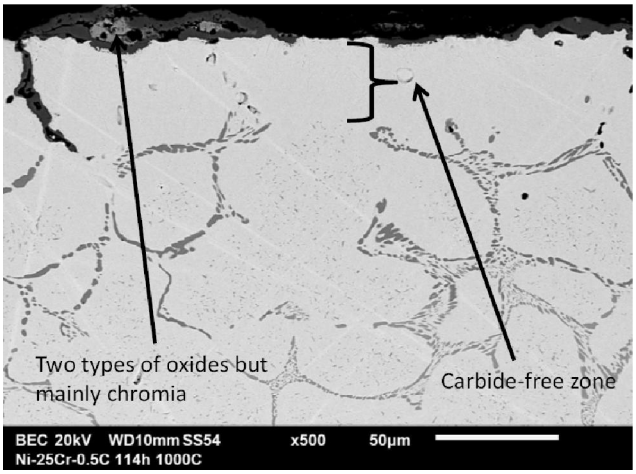

Figure 7 : SEM/BSE micrograph of the oxidized surface observed in cross-section, evidencing two types of external oxides and an outer carbide-free zone

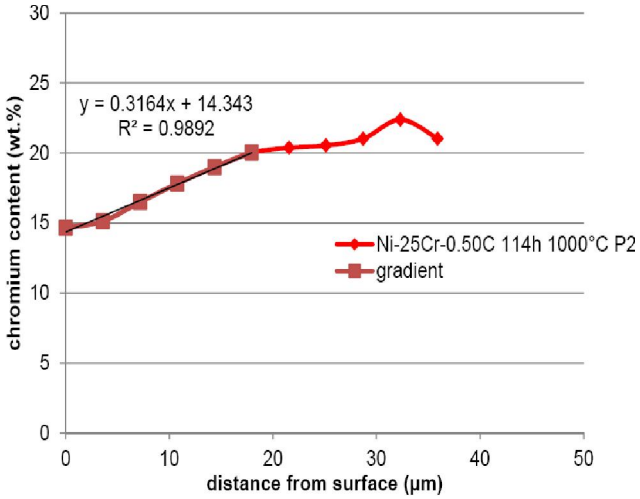

Figure 8 : EDS chromium profile acquired through the Cr-depleted subsurface zone with the SEM

TABLE 3 : Values of the different characteristics resulting from the mass gain exploitation for the whole thermal cycle

Data	Symbol/Formula	Unit
Final isothermal mass gain rate	$\left(\frac{dm}{dt}\right)_{end}$	18.0×10^{-10} g cm^{-2} s^{-1}
Linear constant of chromia volatilization	K_v	19.0×10^{-10} g cm^{-2} s^{-1}
Average gradient of weight content in chromium	$\frac{\Delta WCt_{Cr}}{\Delta h}$	0.3164 wt.%Cr µm^{-1}
Diffusion Coefficient of Chromium at 1000°C through the carbide-free zone	$D_{Cr} = \left(\frac{2 \times M_{Cr}}{3 \times M_O}\right) \times \frac{\left(\frac{dm}{dt}\right)_{end} + K_v}{\rho_{all} \times \frac{\Delta WCt_{Cr}}{\Delta h}}$	2.85×10^{-11} cm^2 s^{-1}

gradient of about 0.316 wt.%Cr µm^{-1} was thus determined.

General commentaries

The value of the finally obtained chromium diffusion coefficient is given in TABLE 3, after the recall of the values of the different experimental data involved in its calculations. This value, which is in good agreement with values of Cr diffusion coefficients earlier obtained at the same temperatures for similar alloys[11,12], well represents the reality of chromium diffusion in situation of oxidation at high temperature of a {chromium carbides}-containing nickel-based alloy since it takes into account the presence of interdendritic spaces perturbed by the initial presence of chromium carbides which dissolved during oxidation. This determination was helped here by the fact that chromia was the predominant oxide, despite the presence of the spinel one which may influence a little the chromium consumption and the overall diffusion. To finish one can underline that it was essential, even at this rather low temperature for which the chromia volatilization is not yet fast, to value the volatilization constant. Indeed this one, which is directly added to the final isothermal mass gain rate, was almost equal to the later one, with as consequence if not taken into account, an underestimation of 50% of the calculated diffusion coefficient. This was so important since, because the rather long duration of the oxidation test (more than 100 hours) allowing a sufficiently deep chromium-depletion (for a good determination of the Cr concentration gradient), the instantaneous mass gain rate has significantly decreased by comparison to its initial value existing at the start of the isothermal stage.

CONCLUSIONS

Thus, the combination of thermogravimetry measurements during high temperature oxidation test with the measurement of the subsurface chromium concentration profile, allows determining the chromium diffusion coefficient of chromium specifically in a zone for which its knowledge is of high importance: the subsurface zone affected by oxidation in the previous instants, crossed by chromium from its origin (matrix remained rich in chromium and chromium carbides existing as Cr-reservoirs in the interdendritic spaces) to the location of its consumption (the external oxide, inner or outer face, this depending on the type of conduction: n or p). If this method – already used in earlier works[11,12] – was possible in the present case (well chromia-forming nickel-based alloy), it will surely more difficult to apply when the oxidation phenomena are more complicated, as in the case of cobalt-based or iron-based which are often not really chromia-forming.

ACKNOWLEDGMENTS

The authors gratefully thank Pascal Villeger for the XRD runs.

REFERENCES

[1] I.S.Kiva, N.G.Kaidash; Soviet Powder Metallurgy and Metal Ceramics, **7(8)**, 635 **(1968)**.
[2] P.Duwez; Powder Met. Bull., **4**, 144 **(1949)**.
[3] M.A.Shtremel; Metal Science and Heat Treatment, **44(7-8)**, 324 **(2002)**.
[4] B.Clausen, K.A.Thorsen; Advances in Powder Metallurgy & Particulate Materials, **4**, 191 **(1992)**.
[5] H.J.Christ, W.Christl, H.G.Sockel; Werkstoffe und Korrosion, **37(7)**, 385 **(1986)**.
[6] H.Inoue, K.Asao, M.Ishio, T.Takasugi; Materials Science Forum, **3442**, 534-543 **(2007)**.
[7] P.Kofstad; 'High Temperature Corrosion', Elsevier applied science, London **(1988)**.
[8] D.Young; 'High Temperature Oxidation and Corrosion of Metals', Elsevier Corrosion Series, Oxford **(2008)**.
[9] C.T.Sims, W.J.Hagel; 'The Superalloys', John Wiley and Sons, New York, **(1972)**.
[10] E.F.Bradley; 'Superalloys: A Technical Guide" (1st edition), ASM International, Metals Park, **(1988)**.
[11] P.Berthod; Oxidation of Metals, **68**, 77 **(2007)**.
[12] P.Berthod, S.Noël, L.Aranda; Annales de Chimie – Science des Matériaux, **33(1)**, 59 **(2008)**.
[13] P.Berthod; Oxidation of Metals, **64(3/4)**, 235 **(2005)**.